PAPER • **OPEN ACCESS**

Hydrodynamic analysis of Remotely Operated Vehicle (ROV) Observation Class using CFD

To cite this article: D Satria *et al* 2019 *IOP Conf. Ser.: Mater. Sci. Eng.* **645** 012014

IOP Conf. Series: Materials Science and Engineering **645** (2019) 012014 doi:10.1088/1757-899X/645/1/012014

Hydrodynamic analysis of Remotely Operated Vehicle (ROV) Observation Class using CFD

D Satria[1,*], R Wiryadinata[2], D P A Esiswitoyo[1], M I Adji[1], I Rosyadi[1], E Listijorini[1], Sunardi[1]

[1]Mechanical Engineering Department, Universitas Sultan Ageng Tirtayasa, Indonesia
[2]Electrical Engineering Department, Universitas Sultan Ageng Tirtayasa, Indonesia

[*] Email: dhimas@untirta.ac.id

Abstract. Remotely Operated Vehicle (ROV) is a small marine craft used for underwater observation. Hence, the analysis of hydrodynamic characteristics is important. Hydrodynamic characteristics can be obtained by fluid dynamic visualization and simulation of *Computational Fluid Dynamic* (CFD). In this paper, ROV Hydrodynamic characteristics begin by forming a three-dimensional (3D) ROV model, forming link elements (mesh) from the 3D ROV model, and forming the computational domain used for CFD simulations. CFD simulations were conducted by analyzing the fluid flow angle variations that represent motion of the ROV, namely translational motion and rotational motion towards the vertical axis (yaw). The simulation results obtained were compared with the previous ROV design that had been developed, so as to obtain an evaluation of the results of the design optimization. The results showed an increase in the hydrodynamic characteristics of the optimal ROV design indicated by the value of drag, pressure distribution, and fluid flow contour.

1. Introduction

The cheapest and easiest water observation method to obtained information about water is by using observation equipment, namely remotely operated vehicle (ROV). In this case, there are several studies to develop ROV as observation equipment with various shapes. Every shapes and design has different hydrodynamic characteristic. The easiest way to obtain hydrodynamic characteristic is by simulation by using software of Computational Fluid Dynamic (CFD) compare to experiment [1,2]. In study of Amjith et al [3], analysis of hydrodynamics characteristic with the consideration of voltage and pressure contour was done by using software of ANSYS. Yue et al [4] used represent of 3 degree freedom of movement from observation to obtain drag coefficient with the software of ANSYS and in term of the deviation value through simulation by manual calculation.

Hydrodynamic analysis in this research aims to obtain hydrodynamic characteristic from developed optimum design of ROV [5], and considered from the comparison both design. Because good geometry can minimize energy required for ROV to move in fluid in determined speed [6]. As a note, the new design of ROV model used in this study (Figure 1) is the result of conceptualization of ROV design of previous design[7]. Therefore it is expected that the hydrodynamic characteristic of optimum design give better character compare to previous design.

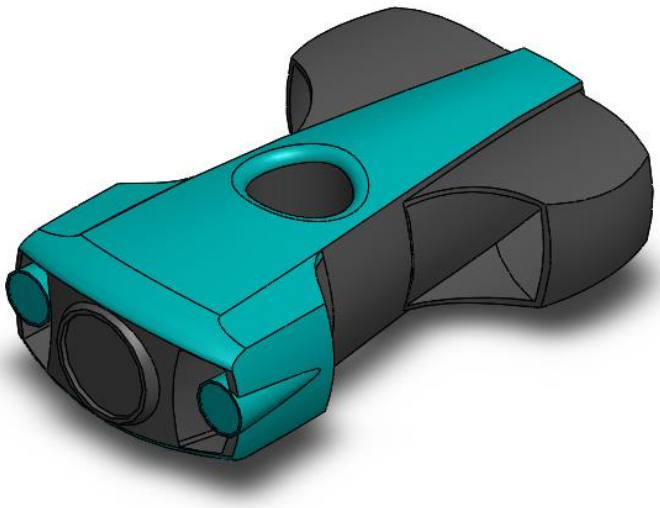

Figure 1. New design of ROV

2. Materials and Methods

Hydrodynamic characteristics can be obtained by fluid dynamic visualization and simulation of *Computational Fluid Dynamic* (CFD). In this paper, ROV Hydrodynamic characteristics begin by forming a three-dimensional (3D) ROV model, forming link elements (mesh) from the 3D ROV model, and forming the computational domain used for CFD simulations.

2.1. Simulation preparation

Simulation was conducted by forming 3D model beforehand from the concept of ROV body. The case of fluid flow in this study was sea wave of Sunda strait, which has the character of incompressible [8,9], open channel, and turbulent because ROV works in open sea water in which the flow is not uniform [8,10]. The solution toward turbulent flow, flow simulation using $k-\varepsilon$ model, which is two equations consist of turbulent kinetic energy and dissipation ratio [11].

The general simulation setting consists of the value of entering the simulation parameters. The wall condition used is the adiabatic wall. Meanwhile the initial and ambient conditions used are pressure and potential pressure P = 999600 Pa, and T = 305.5 K. Assuming that the ROV sinks to a depth of 100 m and move with an average speed $\mathrm{v} = 2\,{}^{\mathrm{m}}/_{\mathrm{s}^2}$.

2.2. Link elements (mesh) and computational domain

Mesh in simulation computation is fully controlled by flow simulation automatically, by simplifying 3D model into mesh model Figure 2 shows the fluid flow *Computational Domain* with the size of the computational field proportional to the size of the ROV. In the computational area it has been shown the fields of in flow, openings, and walls.

This study uses a fixed mesh method, in which it is assumed that the fluid moves at the speed at which the ROV moves and the ROV model is silent (static). Figure 3 shows representation of the motion of the ROV was conducted by changing the slope of the ROV to the direction of fluid flow. Two simulation conditions were used as representations of ROV motion, those are:

- condition 1, the fluid flow rate is parallel to the object that represents heave motion.
- condition 2, variation of the ROV slope towards the direction of the fluid flow rate with a slope variation from 10 ° to 80 ° which represents the diving motion.

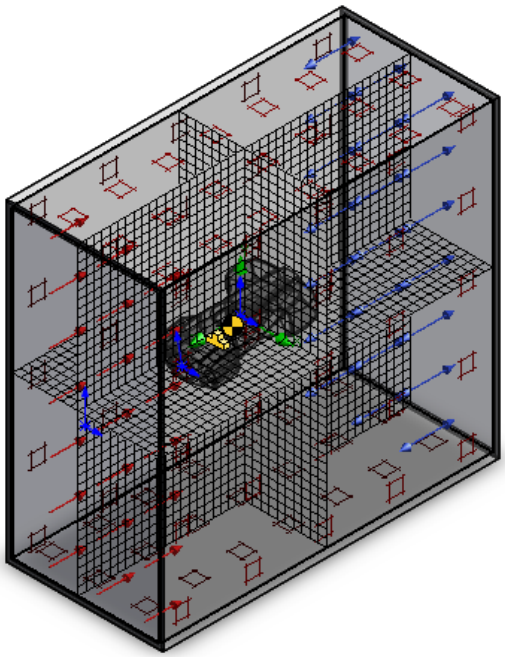

Figure 2. Computational domain and mesh

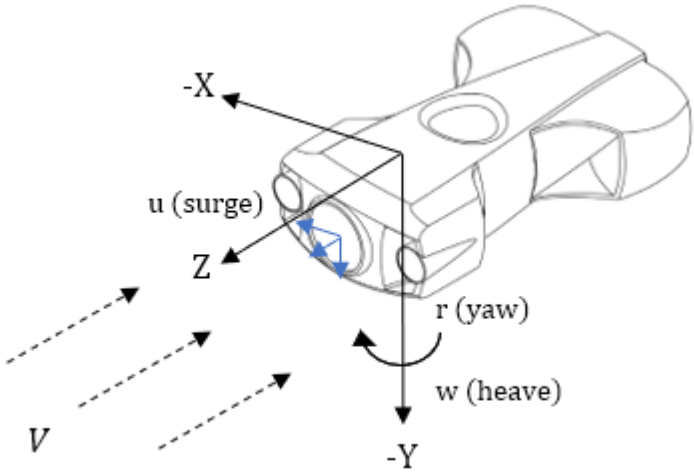

Figure 3. Flow simulation coordinate system

2.3. Simulation objective

The objective of the simulation is to obtain the value of the force and moment generated due to the fluid flow experienced by the ROV body. Tension and moment values are generated from the three static cases of the link element in the three coordinate axes; style values for drag force and lift force, and moment values. The drag coefficient value is also obtained from the objective equation by entering the drag coefficient equation into the simulation.

$$C_d = \frac{F_D}{\rho A \frac{V^2}{2}} \quad (1)$$

3. Result and Discussion

By carrying out objective resolution simulations with mesh and computational fields, and general simulation settings. Simulation forms the results in the form of flow visualization plots and objective plots in the form of values for each iteration. Flow simulation uses the number of iterations as 570-1600 and interval analysis as 120 which is determined automatically by Flow Simulation with consideration of the model geometry and general simulation settings. Mesh and the number of iterations are formed automatically with the algorithm to obtain results that fot to the best abilities and results.

3.1. Simulation convergence

The flow simulation was conducted by using the average formulation of the Navier-Stokes equation so that it is not determined how the software defines convergence. However, the determination of convergence data from the simulation results was determined by variable computing on initialization and boundary conditions, so that the results obtained do not change significantly. From Figure 4, a good residual value is below 1, where the moment on the z-axis and the force on the y-axis have the lowest convergence.

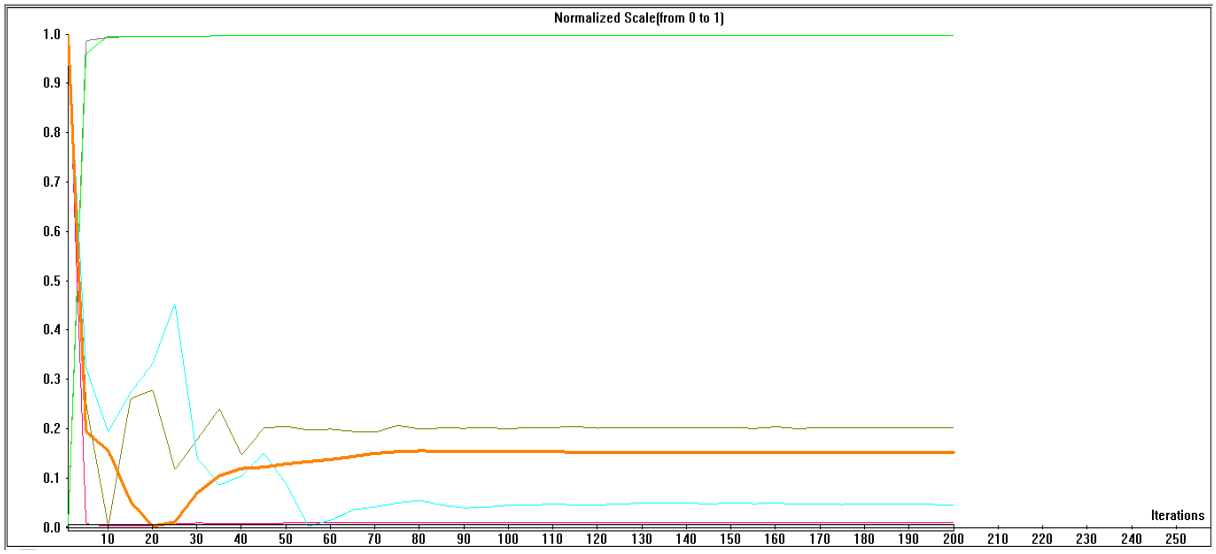

Figure 4. Residual value simulation

3.2. Horizontal motion simulation

ROV moves relatively to the speed of fluid flow and static ROV to the speed of constant fluid flow. Figure 4 is the visualization of fluid flow in speed parameters. The fluid flow profile forms a stagnation area on the front of the ROV. As the result of the stagnation area on the front of the ROV, the speed parameter value has expanded to 2.5m⁄s. The flow tends to degrade from the stagnation area (forebody) to the back of the body with a good profile differentiation. The boundary layer is formed and limits between the surface of the object with an area where viscosity is ignored, has a smooth gradient. The gradient gives a low amount of friction drag. In addition, visualization of flow profiles shows good flow separation, which increases the hydrodynamics of the ROV body.

Variables obtained from the simulation of horizontal translational motion represent the value of the drag force and lift force. The value of drag force and lift force obtained were: -74.15 N and -12911.47 N. The drag force obtained tends to form friction drag because the geometry and wake phenomena resulting from the flow separation tend to be low. The fixed mesh method defines a vector where the fluid v moves in the direction of the negative z-axis with the assumption that it is normalized as a vector to the positive z-axis, which represents the thrust of the thruster. Thus, the value of the drag force and

lift force obtained was negative, which shows the force opposite to the load (load; weight and thrust force) of the ROV.

3.3. Diving motion simulation

ROV slope variation illustrates the motion of diving from the ROV to the critical point of diving capability (90 °), thus the ROV attack angle is varied by changing the slope of the ROV to the fluid flow rate. Other simulation settings use the same values as horizontal translational motion simulations. Figure 5 is a visualization of the fluid flow profile to changes in the slope angle of the ROV. Fluid flow separation due to the asymmetrical ratio of contact surface area and the resulting Eddy motion exacerbates the effect of wake phenomenon so that the drag value increases.

This phenomenon is proven by the force obtained from the simulation of the ROV slope variation and it is displayed in the linear graph that it is gradually increasing to its critical point. Figure 6 shows a graph of the correlation between forces on the z-axis and ROV slope. The graph shows the linearity of the data (shown in the trend line), where the greater the ROV slope angle, the greater the force produced on the z-axis. Linearity of force relationship data with slope is also obtained on the other two axes.

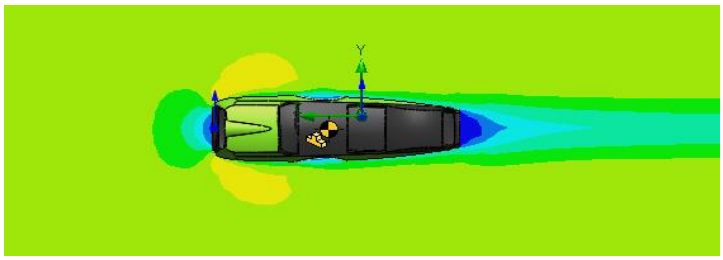

Figure 5. Flow profile of speed profile

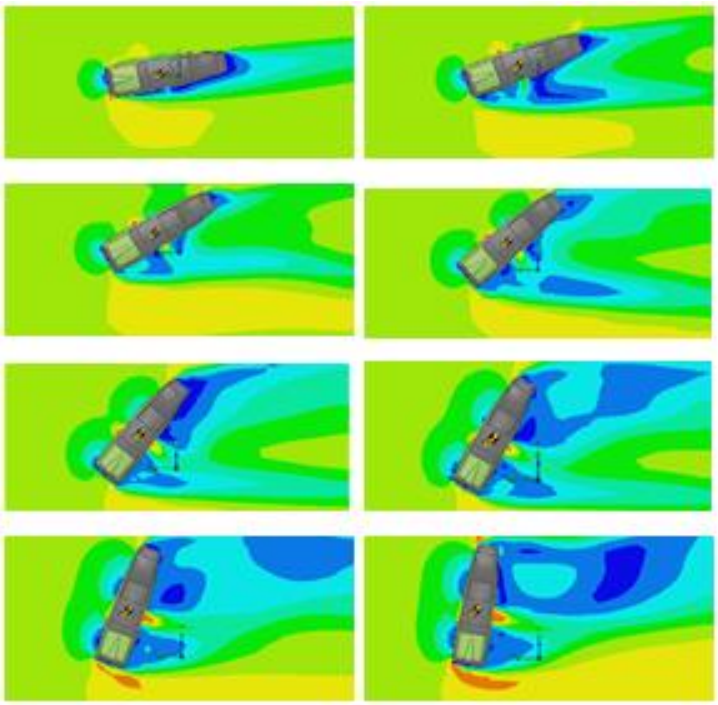

Figure 6. Variation of slope, respectively; 10°, 20°, 30°, 40°, 50°, 60°, 70°, and 80°

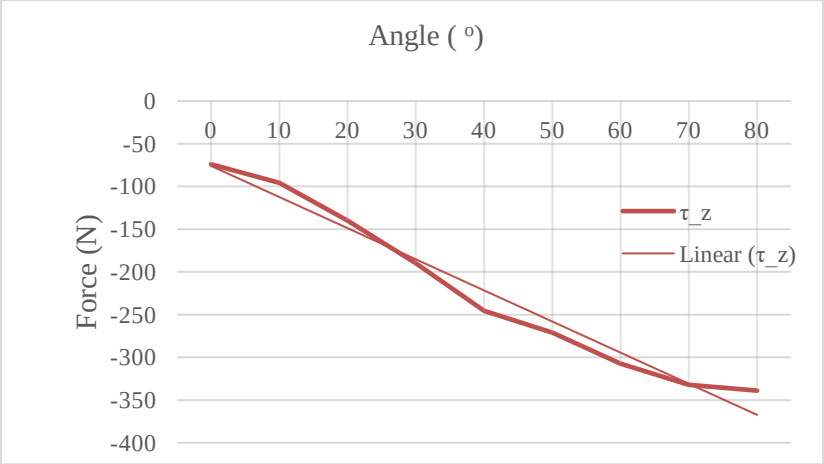

Figure 7. Linearity of drag force value

Figure 7 shows that the greater the slope, the more force the ROV needs to dive. The graph shows negative linear data because the direction of flow velocity is assumed to be normal to the negative z-axis, so the direction of flow velocity is positive. The force on the z-axis due to the load of the fluid flow results in a design resistance that is opposite of the direction of fluid flow Design resistance in this context is the force of the simulation results on the z-axis and y-axis. These conditions in the context of a vector are defined in the opposite direction, or negative. The acquired resistance cannot represent the real dive force. The diving resistance force is obtained from the resultant of the two resistance vectors, to the slope.

The drag force relative to the direction of velocity and lift force is perpendicular to the direction of flow velocity. Resistance on the z-axis and the -y axis is the gait and lift force on the flow direction if it is assumed that the ROV remains in its position. To get the thrust when diving, the consideration of the principle of Archimedes is applied. If it is assumed that the ROV is diving at its slope, the ROV thrust required is the resultant force of resistance to the slope, hydrostatic force on the bottom surface of the ROV (force on the y-axis), and the specific gravity of the ROV and fluid density.

3.4. Comparison of numerical variable design

Numerical hydrodynamic variables as comparative aspects are measured values. Therefore this section compares the values obtained from the simulation results. The first aspect is drag force. As previously mentioned, the two designs use a different form. This difference affects the tendency of the drag force. Old designs tend to form drag and optimal designs tend to form friction drag. The drag force of the old design obtained from the simulation was 88.13 N while the drag force of the optimal design is 74.15 N. There is a large increase in resistance or the drag force in the optimal design as 18.8%. From the drag force can be calculated the drag coefficient of the two designs.

Variables that need to be determined to obtain the drag coefficient are the contact surface area. Contact surface area is measured from the 3D design model. The contact surface area for the old design was $A_l = 0.028\ m^2$ and the optimal design of $A_o = 0.040\ m^2$. Then the drag coefficient was obtained as follow:

$$C_{d_l} = \frac{2 \times 88{,}13\ N}{1020\ {}^{kg}/_{m^3} \times (2\ {}^{m}/_{s})^2 \times 0{,}070} = 1{,}60$$

$$C_{d_o} = \frac{2 \times 74{,}15\ N}{1020\ {}^{kg}/_{m^3} \times (2\ {}^{m}/_{s})^2 \times 0{,}040} = 0{,}91$$

The calculation of the drag coefficient theory of both designs shows a significant difference between the old design and the optimal design. The old design has a drag coefficient value of $C_{d_l} = 1{,}60$ and the optimal design has a drag coefficient of $C_{d_o} = 0{,}91$. The increase in drag coefficient was 43% from the optimization results. Comparison of the free variable drag coefficient between the old design and the optimal design was 1:2. The greater the ratio of the independent variable (drag force versus the area of contact area) the better the value of drag coefficient would be. In addition to the comparison between the independent variables, the old design fluid flow separation forms a fairly large wake area with a pressure reduction value which was 612.10 Pa from an environmental dynamic pressure as 2448.20 Pa.

4. Conclusion

Hydrodynamic analysis in this research aims to obtain hydrodynamic characteristic from developed optimum design of ROV. The result shows an increase in the hydrodynamic characteristics of the optimal ROV design indicated by the value of drag, pressure distribution, and fluid flow contour. The old design has a drag coefficient value of $C_{d_l} = 1{,}60$ and the optimal design has a drag coefficient of $C_{d_o} = 0{,}91$. The increase in drag coefficient from the optimization result is 43% .

Acknowledgments

The authors would like to send the gratitude to the Directorate of Research and Community Service (DRPM) of DIKTI who has funded this research in the 2018.

References

[1] J. Ramirez-Macias, P. Brongers, S. Rua, and R. . Vasquez, "Hydrodynamic modelling for the remotely operated vehicle Visor3 using CFD," *IFAC-PapersOnLine 49-23*, pp. 187–192, 2016.

[2] H. Zhang, "Using CFD Software to Calculate Hydrodynamic Coefficients," *Mar. Sci. Appl.*, vol. 9, pp. 149–155, 2010.

[3] K. Amjith, V. Arundas, M. Harikrishnan, J. Sebastian, and V. Vineeth, "Underwater Search and Rescue Device," *Int. J. Innov. Res. Sci. Technol.*, vol. 1, no. 11, pp. 481–488, 2015.

[4] C. Yue, "ANSYS FLUENT-Based Modeling and Hydrodynamic Analysis for a Spherical Underwater Robot," *IEEE Int. Conf. Mechatronics Autom.*, vol. 13, pp. 1577–1581, 2013.

[5] R. Wiryadinata, A. S. Nurliany, I. Muttakin, and T. Firmansyah, "Design of a Low Cost Remotely Operated Vehicle with 3 DoF Navigation," *Bull. Electr. Eng. Informatics*, vol. 6, no. 1, pp. 13–23, 2017.

[6] D. L. Paster, "Importance of Hydrodynamic Considerations for Underwater Vehicle Design," *IEEE*, pp. 1413–1422, 1986.

[7] D. Satria, D. P. A. L. Esiswitoyo, N. K. Caturwati, E. Listijorini, and R. Lusiani, "Body Design Concept of Remotely Operated Vehicle (ROV) of Observation Class with the Method of Concept Screening and Concept Scoring," in *MATEC Web Conf. Volume 218, 02009, The 1st International Conference on Industrial, Electrical and Electronics (ICIEE 2018)*, 2018.

[8] Y. . Cengel, *Fundamental of Fluid Mechanics*. New York: McGraw-Hill, 2006.

[9] D. Satria, Haryadi, R. Austin, and B. Kurniawan, "Design of drying chamber and biomass furnace for sun-biomass hybrid rice-drying machine," *AIP Conf. Proc.*, vol. 1717, 2016.

[10] T. I. Fossen, *Handbook of Marine Craft Hydrodynamics and Motion Control*. Trondheim: John Wiley & Sons Publication, 2011.

[11] H. . Versteeg, *An Introduction to Computational Fluid Dynamics: The Finite Volume Method*. Pearson Education Limited, 2007.